

Scaling Tests of the Cross Section for Deeply Virtual Compton Scattering

C. Muñoz Camacho,¹ A. Camsonne,² M. Mazouz,³ C. Ferdi,² G. Gavalian,⁴ E. Kuchina,⁵ M. Amarian,⁴ K. A. Aniol,⁶ M. Beaumel,¹ H. Benaoum,⁷ P. Bertin,^{2,8} M. Brossard,² J.-P. Chen,⁸ E. Chudakov,⁸ B. Craver,⁹ F. Cusanno,¹⁰ C.W. de Jager,⁸ A. Deur,⁸ R. Feuerbach,⁸ J.-M. Fieschi,² S. Frullani,¹⁰ M. Garçon,¹ F. Garibaldi,¹⁰ O. Gayou,¹¹ R. Gilman,⁵ J. Gomez,⁸ P. Gueye,¹² P.A.M. Guichon,¹ B. Guillon,³ O. Hansen,⁸ D. Hayes,⁴ D. Higinbotham,⁸ T. Holmstrom,¹³ C.E. Hyde-Wright,⁴ H. Ibrahim,⁴ R. Igarashi,¹⁴ X. Jiang,⁵ H.S. Jo,¹⁵ L. Kaufman,¹⁶ A. Kelleher,¹³ A. Kolarkar,¹⁷ G. Kumbartzki,⁵ G. Laveissiere,² J.J. LeRose,⁸ R. Lindgren,⁹ N. Liyanage,⁹ H.-J. Lu,¹⁸ D.J. Margaziotis,⁶ Z.-E. Meziani,¹⁹ K. McCormick,⁵ R. Michaels,⁸ B. Michel,² B. Moffit,¹³ P. Monaghan,¹¹ S. Nanda,⁸ V. Nelyubin,⁹ M. Potokar,²⁰ Y. Qiang,¹¹ R.D. Ransome,⁵ J.-S. Réal,³ B. Reitz,⁸ Y. Roblin,⁸ J. Roche,⁸ F. Sabatié,¹ A. Saha,⁸ S. Sirca,²⁰ K. Slifer,⁹ P. Solvignon,¹⁹ R. Subedi,²¹ V. Sulkosky,¹³ P.E. Ulmer,⁴ E. Voutier,³ K. Wang,⁹ L.B. Weinstein,⁴ B. Wojtsekowski,⁸ X. Zheng,²² and L. Zhu²³

(The Jefferson Lab Hall A Collaboration)

¹CEA Saclay, DAPNIA/SPhN, F-91191 Gif-sur-Yvette, France

²Université Blaise Pascal/CNRS-IN2P3, F-63177 Aubière, France

³Laboratoire de Physique Subatomique et de Cosmologie, 38026 Grenoble, France

⁴Old Dominion University, Norfolk, Virginia 23508, USA

⁵Rutgers, The State University of New Jersey, Piscataway, New Jersey 08854, USA

⁶California State University, Los Angeles, Los Angeles, California 90032, USA

⁷Syracuse University, Syracuse, New York 13244, USA

⁸Thomas Jefferson National Accelerator Facility, Newport News, Virginia 23606, USA

⁹University of Virginia, Charlottesville, Virginia 22904, USA

¹⁰INFN/Sezione Sanità, 00161 Roma, Italy

¹¹Massachusetts Institute of Technology, Cambridge, Massachusetts 02139, USA

¹²Hampton University, Hampton, Virginia 23668, USA

¹³College of William and Mary, Williamsburg, Virginia 23187, USA

¹⁴University of Saskatchewan, Saskatchewan, SK, Canada, S7N 5C6

¹⁵Institut de Physique Nucléaire CNRS-IN2P3, Orsay, France

¹⁶University of Massachusetts Amherst, Amherst, Massachusetts 01003, USA

¹⁷University of Kentucky, Lexington, Kentucky 40506, USA

¹⁸Department of Modern Physics, University of Science and Technology of China, Hefei 230026, China

¹⁹Temple University, Philadelphia, Pennsylvania 19122, USA

²⁰Institut Jozef Stefan, University of Ljubljana, Ljubljana, Slovenia

²¹Kent State University, Kent, Ohio 44242, USA

²²Argonne National Laboratory, Argonne, Illinois, 60439, USA

²³University of Illinois, Urbana, Illinois 61801, USA

We present the first measurements of $\vec{e}p \rightarrow e p \gamma$ cross section in the deep virtual Compton scattering (DVCS) regime and the valence quark region ($x_{Bj} = 0.36$). From JLab E00-110, we extract the imaginary part of the Bethe-Heitler (BH)-DVCS interference terms, to order twist-3 for $Q^2 = 1.5$, 1.9, and 2.3 GeV 2 , and the real part of the BH-DVCS interference terms at $Q^2 = 2.3$ GeV 2 . We present the first model-independent measurement of linear combinations of generalized parton distributions (GPDs) and GPD integrals up to twist-3 approximation. The validity of this approximation is strongly supported by the absence of Q^2 -variation of the extracted terms – thereby constraining the size of higher twist contributions to our observables.

PACS numbers: 13.60.Fz, 13.40.Gp, 14.20.Dh, 13.60.Hb

Understanding nucleon structure is a primary goal of nuclear physics today. Measurements of electro-weak form factors determine nucleon spatial structure, and deep inelastic scattering (DIS) of leptons off the nucleon measures parton distribution functions, which determine longitudinal momentum distributions. The demonstration by Ji [1], Radyushkin [2], and Müller *et al.* [3], of a formalism to relate the spatial and momentum distributions of the partons allows the exciting possibility of determining spatial distributions of quarks and gluons

in the nucleon as a function of the parton wavelength. These new structure functions, now called generalized parton distributions (GPD), became of experimental interest when it was shown [1] that they are accessible through deep virtual Compton scattering (DVCS) and its interference with the Bethe-Heitler (BH) process (Fig. 1). Fig. 1 presents our kinematic nomenclature. DVCS is defined kinematically by the limit $-t \ll Q^2$ and Q^2 much larger than the quark confinement scale.

The factorization proofs [4, 5] confirmed the connec-

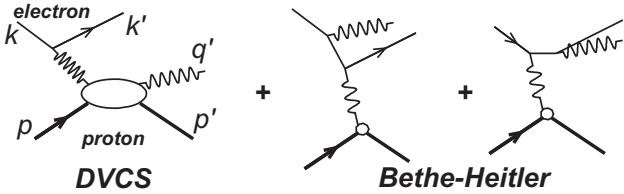


FIG. 1: Lowest-order QED diagrams for the process $ep \rightarrow ep\gamma$, including the DVCS and Bethe-Heitler (BH) amplitudes. The external momentum four-vectors are defined on the diagram. The virtual photon momenta are $q = k - k'$ in the DVCS- and $\Delta = q - q'$ in the BH-amplitudes. The invariants are: $W^2 = (q+p)^2$, $Q^2 = -q^2 > 0$, $t = \Delta^2$, $x_{Bj} = Q^2/(2p \cdot q)$, and the DVCS scaling variable $\xi = -\bar{q}^2/(\bar{q} \cdot P) \approx x_{Bj}/(2-x_{Bj})$, with $\bar{q} = (q+q')/2$ and $P = p+p'$.

Kin	k' (GeV/c)	θ_e ($^{\circ}$)	Q^2 (GeV 2)	x_{Bj}	θ_q ($^{\circ}$)	W (GeV)	$q'(0^{\circ})$ (GeV/c)
1	3.53	15.6	1.5	0.36	-22.3	1.9	2.14
2	2.94	19.3	1.9	0.36	-18.3	2.0	2.73
3	2.34	23.8	2.3	0.36	-14.8	2.2	3.33

TABLE I: Experimental $ep \rightarrow ep\gamma$ kinematics, for incident beam energy $E = 5.75$ GeV. θ_q is the central value of the \mathbf{q} -vector direction. The PbF_2 calorimeter was centered on θ_q for each setting. The photon energy for $\mathbf{q}' \parallel \mathbf{q}$ is denoted $q'(0^{\circ})$.

tion between DVCS and DIS. Diehl *et al.* [6] showed that the twist-2 and twist-3 contributions in the DVCS-BH interference terms (the first two leading orders in a $1/\sqrt{Q^2}$ expansion) could be extracted independently from the azimuthal-dependence of the helicity-dependent cross section. Burkardt [7] showed that the t -dependence of the GPDs is the Fourier conjugate to the transverse spatial distribution of quarks in the infinite momentum frame as a function of momentum fraction. Diehl [8] and Belitsky *et al.* [9] extended this interpretation to the general case of skewness $\xi \neq 0$.

These elegant theoretical concepts stimulated an intense experimental effort in DVCS. The H1 [10, 11] and ZEUS [12] collaborations at HERA measured the cross section for $x_{Bj} \approx 2\xi \approx 10^{-3}$. The HERMES collaboration measured relative beam-helicity [13] and beam-charge asymmetries [14, 15]. Relative beam-helicity [16] and longitudinal target [17] asymmetries were also measured at the Thomas Jefferson National Accelerator Facility (JLab) by the CLAS collaboration.

We initiated E00-110 in Hall A at JLab to obtain cross section measurements with good control of exclusivity to test the hypothesis of twist-2 dominance in the kinematics accessible with 6 GeV electrons. We report here the measurement of the cross section of the $\bar{e}p \rightarrow ep\gamma$ reaction for positive and negative electron helicity in the

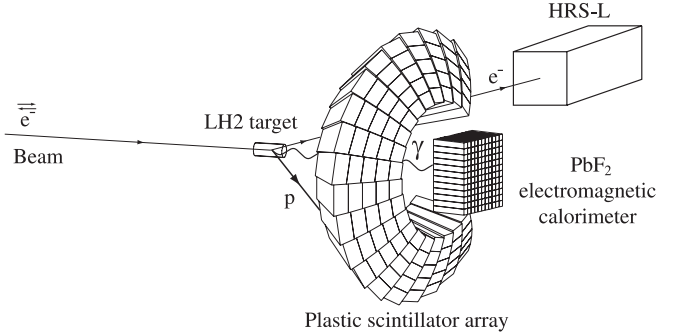


FIG. 2: Experimental configuration for the DVCS experiment in JLab Hall A. Electrons scattered from the liquid H_2 target are detected in the HRS-L. Photons are detected in the PbF_2 calorimeter. A sample of protons are detected in the scintillator array.

kinematics of Table I. Fig. 1 illustrates the lowest-order QED diagrams for this process.

Our data were acquired in JLab Hall A [18] (Fig. 2). The 5.75 GeV electron beam was incident on a 15 cm liquid H_2 target. Our typical luminosity was $10^{37}/\text{cm}^2/\text{s}$ with 76% beam polarization. We detected the scattered electrons in the left (as viewed from the beam) High Resolution Spectrometer (HRS-L). With the use of detectors with direct view of the target at high luminosity, we took care to minimize background and absorption processes in the target and surrounding material. We built a new vacuum chamber surrounding the liquid hydrogen target, with a spherical form of radius 63 cm and of wall thickness 1 cm Al. The windowless exit beam pipe joined this sphere with an expanded 13 cm circular inner aperture flaring to match the standard downstream beam pipe at 2 m. A thin window faced the entrance window of the HRS-L. Photons (and $\gamma\gamma$ coincidences from π^0 decay) were detected in a 11×12 array of $3 \times 3 \times 18.6 \text{ cm}^3$ PbF_2 crystals, whose front face was located 110 cm from the target center. The PMT signals from the PbF_2 elements were digitized by a 128 sample \times 1GHz waveform digitizer, based on the Analog Ring Sampler (ARS) memory chip [19]. A passive splitter also sent each PbF_2 signal to a digital trigger-validation circuit. A standard electron trigger from the HRS-L stopped the ARS acquisition and triggered a programmable width (typically 60 ns) sample-and-hold (SH) integration and digitization on each PbF_2 channel in the digital trigger. The trigger then computed all overlapping 2×2 cluster sums. If no sum was found over a programmable threshold set to 1 GeV equivalent, all ARS and SH buffers were cleared and acquisition restarted. This validation-reset cycle has a 500 ns deadtime. When the trigger found cluster(s) above threshold, all signals in the corresponding ARS channels were digitized and recorded for that event, together with the HRS information. We calibrated the

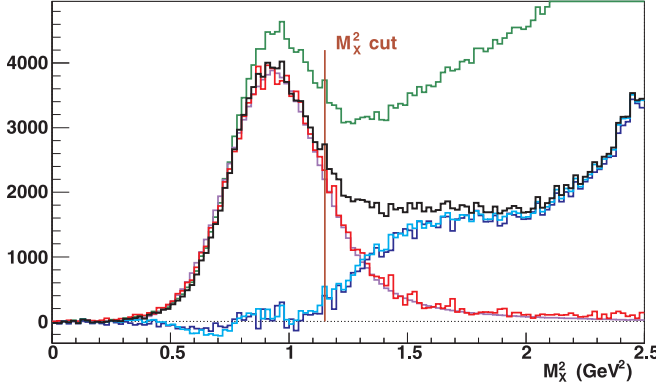


FIG. 3: Missing mass squared for $H(e, e'\gamma)X$ events (green curve) at $Q^2 = 2.3$ GeV 2 and $-t \in [0.12, 0.4]$ GeV 2 , integrated over the azimuthal angle of the photon $\phi_{\gamma\gamma}$. The black curve shows the data once the $H(e, e'\gamma)\gamma X'$ events have been subtracted. The other curves are described in the text.

PbF₂ array by coincident elastic $H(e, e'_{\text{Calo}}p_{\text{HRS}})$ data. With (elastic) $k' = 4.2$ GeV/c, we obtain a PbF₂ resolution of 2.4% in energy and 2 mm in transverse position (one- σ). The calibration was monitored during the experiment by intermittent blue LED scans and by reconstruction of the $\pi^0 \rightarrow \gamma\gamma$ mass from $H(e, e'\pi^0)X$ events. Offline analysis of the ARS waveforms for each channel allowed us to maintain this resolution, even with accidental pileup pulses separated by as little as 4 ns.

We present in Fig. 3 the missing mass squared obtained for $H(e, e'\gamma)X$ events, with coincident electron-photon detection. After subtraction of an accidental coincidence sample, our data is essentially background free: we have negligible contamination of non-electromagnetic events in the HRS and PbF₂ spectra. In addition to $H(e, e'\gamma)p$, however, we do have the following competing channels: $ep \rightarrow e\pi^0p$, $ep \rightarrow e\pi^0N\pi$, $ep \rightarrow e\gamma N\pi$, $ep \rightarrow e\gamma N\pi\pi\dots$. From symmetric (lab-frame) π^0 -decay, we obtain a high statistics sample of $H(e, e'\pi^0)X'$ events, with two photon clusters in the PbF₂ calorimeter. From these events, we determine the statistical sample of [asymmetric] $H(e, e'\gamma)\gamma X'$ events that must be present in our $H(e, e'\gamma)X$ data. The M_X^2 spectrum displayed in black in Fig. 3 was obtained after subtracting this π^0 yield from the total (green) distribution. This is a 14% average subtraction in the exclusive window defined by 'M_X² cut' in Fig. 3. Depending on the bin in $\phi_{\gamma\gamma}$ and t , this subtraction varies from 6% to 29%. The result shows a clear exclusive peak with a shoulder from threshold- $N\pi$ and Δ production, and a continuum rise above the $H(e, e'\gamma)N\pi\pi\dots$ threshold. After our π^0 subtraction, the only remaining channels, of type $H(e, e'\gamma)N\pi$, $N\pi\pi$, *etc.* are kinematically constrained to $M_X^2 > (M + m_\pi)^2$. This is the value ('M_X² cut' in Fig. 3) we chose for truncating our integration. Resolution effects can cause the inclusive channels to contribute be-

low this cut. To evaluate this possible contamination, we used an additional proton array (PA) of 100 plastic scintillators. The PA subtended a solid angle (relative to the nominal direction of the \mathbf{q} -vector) of $18^\circ < \theta_{\gamma p} < 38^\circ$ and $45^\circ < \phi_{\gamma p} = 180^\circ - \phi_{\gamma\gamma} < 315^\circ$, arranged in 5 rings of 20 detectors. For $H(e, e'\gamma)p$ events near the exclusive region, we can predict which block in the PA should have a signal from a proton from an exclusive $H(e, e'\gamma)p$ event. The red histogram is the $X = (p + y)$ missing mass squared distribution for $H(e, e'\gamma)p$ events in the predicted PA block, with a signal above an effective threshold 30 MeV (electron equivalent). The blue curve shows our inclusive yield, obtained by subtracting the normalized triple coincidence yield from the $H(e, e'\gamma)X$ yield. The (smooth) violet curve shows our simulated $H(e, e'\gamma)p$ spectrum, including radiative and resolution effects, normalized to fit the data for $M_X^2 \leq M^2$. The cyan curve is the estimated inclusive yield obtained by subtracting the simulation from the data. The blue and cyan curves are in good agreement, and show that our exclusive yield has less than 3% contamination from inclusive processes.

The following equations reproduce the consistent expansion of the DVCS cross section to order twist-3 of Belitsky, Müller, and Kirchner [20]. The azimuthal angle $\phi_{\gamma\gamma}$ of the detected photon is defined in a right-handed coordinate system with $\hat{z}_q = \hat{\mathbf{q}}$ and \hat{y}_q parallel to $\mathbf{k} \times \mathbf{k}'$. This definition of $\phi_{\gamma\gamma}$ agrees with the “Trento-Convention” for ϕ [21], and is the definition used in [13] and [16]. Note that this azimuth convention differs from [20] by $\phi_{\gamma\gamma} = \pi - \phi_{[20]}$. In the following expressions, we utilize the differential phase space element $d^5\Phi = dQ^2 dx_{\text{Bj}} d\phi_e dt d\phi_{\gamma\gamma}$. The helicity-dependent ($d\Sigma$) and helicity-independent ($d\sigma$) cross sections, are:

$$\begin{aligned} \frac{d^5\Sigma}{d^5\Phi} &= \frac{1}{2} \left[\frac{d^5\sigma^+}{d^5\Phi} - \frac{d^5\sigma^-}{d^5\Phi} \right] \\ &= \sin(\phi_{\gamma\gamma}) \Gamma_1^{\Re} \Im \left[\mathcal{C}^I(\mathcal{F}) \right] \\ &\quad - \sin(2\phi_{\gamma\gamma}) \Gamma_2^{\Re} \Im \left[\mathcal{C}^I(\mathcal{F}^{\text{eff}}) \right] \\ &\quad + \frac{d^5\Sigma(|DVCS|^2)}{d^5\Phi} \end{aligned} \quad (1)$$

$$\begin{aligned} \frac{d^5\sigma}{d^5\Phi} &= \frac{1}{2} \left[\frac{d^5\sigma^+}{d^5\Phi} + \frac{d^5\sigma^-}{d^5\Phi} \right] \\ &= \frac{d^5\sigma(|BH|^2)}{d^5\Phi} + \frac{d^5\sigma(|DVCS|^2)}{d^5\Phi} \\ &\quad + \Gamma_0^{\Re} \Re \left[\mathcal{C}^I(\mathcal{F}) \right] + \Gamma_{0,\Delta}^{\Re} \Re \left[\mathcal{C}^I + \Delta \mathcal{C}^I \right] (\mathcal{F}) \\ &\quad - \cos(\phi_{\gamma\gamma}) \Gamma_1^{\Re} \Re \left[\mathcal{C}^I(\mathcal{F}) \right] \\ &\quad + \cos(2\phi_{\gamma\gamma}) \Gamma_2^{\Re} \Re \left[\mathcal{C}^I(\mathcal{F}^{\text{eff}}) \right] \end{aligned} \quad (2)$$

The $\Gamma_n^{\Re, \Im}$ are kinematic factors which depend on x_{Bj} , Q^2 , t , $\phi_{\gamma\gamma}$, and $s = (k + p)^2$. Their $\phi_{\gamma\gamma}$ dependence arises from the electron propagators of the BH amplitude. The \mathcal{C}^I and $\Delta \mathcal{C}^I$ amplitudes are the angular harmonic terms defined in Eqs. 69 and 72 of [20] (we have suppressed the

subscript ‘‘unp’’ since our measurements are only with an unpolarized target). These angular harmonics depend on the interference of the BH amplitude with the set $\mathcal{F} = \{\mathcal{H}, \mathcal{E}, \tilde{\mathcal{H}}, \tilde{\mathcal{E}}\}$ of twist-2 Compton form factors (CFFs) or the related set \mathcal{F}^{eff} of effective twist-3 CFFs:

$$\begin{aligned} \mathcal{C}^I(\mathcal{F}) &= F_1(t)\mathcal{H}(\xi, t) + \xi G_M(t)\tilde{\mathcal{H}}(\xi, t) \\ &\quad - \frac{t}{4M^2}F_2(t)\mathcal{E}(\xi, t) \end{aligned} \quad (3)$$

$$\begin{aligned} \mathcal{C}^I(\mathcal{F}^{\text{eff}}) &= F_1(t)\mathcal{H}^{\text{eff}}(\xi, t) + \xi G_M(t)\tilde{\mathcal{H}}^{\text{eff}}(\xi, t) \\ &\quad - \frac{t}{4M^2}F_2(t)\mathcal{E}^{\text{eff}}(\xi, t) \end{aligned} \quad (4)$$

$$\begin{aligned} [\mathcal{C}^I + \Delta\mathcal{C}^I](\mathcal{F}) &= F_1(t)\mathcal{H}(\xi, t) - \frac{t}{4M^2}F_2(t)\mathcal{E}(\xi, t) \\ &\quad - \xi^2 G_M(t)[\mathcal{H}(\xi, t) + \mathcal{E}(\xi, t)]. \end{aligned} \quad (5)$$

Note that $[\mathcal{C}^I + \Delta\mathcal{C}^I]$ depends only on \mathcal{H} and \mathcal{E} . The usual proton elastic form factors, F_1 , F_2 and $G_M = F_1 + F_2$ are defined to have negative arguments in the space-like regime. The Compton form factors are defined in terms of the vector GPDs H_f and E_f , and the axial vector GPDs \tilde{H}_f and \tilde{E}_f , defined for each flavor of quark f . For example ($f \in \{u, d, s\}$) [20]:

$$\begin{aligned} \mathcal{H}(\xi, t) &= \sum_f \left[\frac{e_f}{e} \right]^2 \left\{ i\pi [H_f(\xi, \xi, t) - H_f(-\xi, \xi, t)] \right. \\ &\quad \left. + \mathcal{P} \int_{-1}^{+1} dx \left[\frac{2x}{\xi^2 - x^2} \right] H_f(x, \xi, t) \right\}. \end{aligned} \quad (6)$$

Twist-3 CFFs contain Wandzura-Wilzcek terms, determined by the twist-2 matrix elements, and dynamic antiquark-gluon-quark twist-3 matrix elements. The twist-2 and twist-3 CFFs are matrix elements of quark-gluon operators and are independent of Q^2 (up to logarithmic QCD evolution). The kinematic suppression of the twist-3 (and higher) terms is expressed in powers of $-t/Q^2$ and $(t_{\min} - t)/Q^2$ in the Γ factors. Also, the twist-3 terms couple to the longitudinal polarization of the virtual photon. The ‘DVCS²’ terms in both $d\sigma$ and $d\Sigma$ are kinematically suppressed by at least an order of magnitude in our kinematics [20], because they are not enhanced by the BH amplitude. For $d\Sigma$, the ‘DVCS²’ term is the conventional LT' term: it is a twist-3-twist-2 interference and therefore has an additional kinematic suppression. We neglect the DVCS² terms in our analysis. The helicity-independent cross section also has a $\cos(3\phi_{\gamma\gamma})$ twist-2 gluon transversity term. We expect this term to be small, and do not include it in our analysis. In any case, the terms we neglect do not affect the cross sections we extract, which are accurately parametrized, within statistics, by the contributions included in our analysis.

In our simulation, we generate events uniformly in a fixed electron phase space $\Delta^3\Phi_e = \Delta Q^2 \Delta x_{\text{Bj}} \Delta\phi_e$ and in a photon phase space $\Delta^2\Phi_\gamma = 2\pi[t_{\min}(Q^2, x_{\text{Bj}}) - t_{\max}]$.

The bound $t_{\max} = -1$ GeV² is an arbitrarily fixed upper bound, and $t_{\min} \approx -x_{\text{Bj}}^2 M^2 / [1 - x_{\text{Bj}}]$ is the event-by-event kinematic upper bound on $t < 0$. We simulate internal bremsstrahlung in the scattering process and external bremsstrahlung and ionization straggling in the target and scattering chamber windows. We include spectrometer resolution and acceptance effects and a full GEANT3 simulation of the detector response to the DVCS photons and protons. The spectrometer acceptance is defined for both the data and simulation by a R -function cut [22]. Radiative corrections for virtual photons and unresolved real photons are applied according to the VCS (BH+Born amplitude) specific prescriptions of Ref. [23]. This results in a global correction factor (independent of $\phi_{\gamma\gamma}$ or helicity) of 0.91 ± 0.02 applied to our experimental yields. Within the quoted uncertainty, this correction is independent of the kinematic setting.

Each kinematic setting has one (Q^2, x_{Bj}) -bin, four t -bins, and 24 $\phi_{\gamma\gamma}$ -bins. For each (Q^2, x_{Bj}, t) bin, we fit the $\Re e$ and $\Im m$ parts (as appropriate) of the harmonics $\mathcal{C}_n \in \{\mathcal{C}^I(\mathcal{F}), \mathcal{C}^I(\mathcal{F}^{\text{eff}}), [\mathcal{C}^I + \Delta\mathcal{C}^I](\mathcal{F})\}$ as independent parameters. We minimize:

$$\chi^2 = \sum_i \left[\left(Y_i^{\text{Exp}} - Y_i^{\text{Fit}} \right)^2 / \sigma_i^2 \right]. \quad (7)$$

The Y_i^{Exp} are the experimental yields, after accidental and π^0 subtractions, in bin i , with statistical errors σ_i . The fit yields, $Y_i^{\text{Fit}} = \sum_n \mathcal{C}_n K_n(i)$, depend linearly on the fitting harmonics \mathcal{C}_n and the Monte-Carlo integrated kinematic weights:

$$K_n(i) = \mathcal{L} \sum_{j=1}^{N^{\text{sim}}} \frac{\Delta^3\Phi_e \Delta^2\Phi_\gamma(j)}{N^{\text{sim}}} \Gamma_n(j) \eta(i, j). \quad (8)$$

\mathcal{L} is the integrated experimental luminosity and N^{sim} is the total number of events in the simulation. The indicator function $\eta(i, j) = 1$ if simulation event j lands in experimental bin i , otherwise, $\eta(i, j) = 0$. After fitting the harmonics \mathcal{C}_n to our experimental yields, we extract the experimental cross section (and associated error bars)

$$\frac{d^5\sigma^{\text{Exp}}(i)}{d^5\Phi} = \frac{d^5\sigma^{\text{Fit}}(i)}{d^5\Phi} Y_i^{\text{Exp}} / Y_i^{\text{Fit}}, \quad (9)$$

where $d^5\sigma^{\text{Fit}}$ is defined by our fitted parameters and Eqs. (1–2).

In Kin-1 and Kin-2, due to the lower q' momenta (Table I), our acceptance, trigger, and readout did not record a comprehensive set of $ep \rightarrow e\pi^0 X$ events. For those events we were able to reconstruct, we found only a few percent contribution to $d\Sigma$, but a larger contribution to $d\sigma$. For Kin-1,2, we only present results on $d\Sigma$. Our systematic errors in the cross-section measurements are dominated by the following contributions: 3% from HRS×PbF₂ acceptance and luminosity; 3% from

$H(e, e'\gamma)\gamma X(\pi^0)$ background; 2% from radiative corrections; and 3% from inclusive $H(e, e'\gamma)N\pi\dots$ background. The total, added in quadrature, is 5.6%. The $d\Sigma$ results contain an additional 2% systematic uncertainty from the beam polarization measurement by the Compton Polarimeter [24]. In order to compute the BH contribution in the $d\sigma$ analysis we used Kelly's parametrization of form factors [25], which reproduce elastic cross-section world data in our t range with 1% error and 90% CL.

For one (Q^2, x_{Bj}, t) bin, Fig. 4 shows the helicity-dependent and helicity-independent cross sections, respectively. Table II lists the extracted angular harmonics. The twist-3 terms make only a very small contribution to our cross sections. The suppression of the twist-3 term \mathcal{F}^{eff} is contained in the kinematic coefficient $\Gamma_2^{\Re, \Im}$ (rather than in the extracted values) and is reflected in the much larger statistical error. The 'DVCS²' terms generate a similar $\phi_{\gamma\gamma}$ -dependence as the BH-DVCS interference terms in the DVCS cross sections $d\Sigma$ and $d\sigma$, and cannot be extracted independently. Thus the angular harmonic terms in Table II may include contributions from bilinear 'DVCS²' terms omitted in our analysis. However, as noted above, these terms are suppressed kinematically, especially in the cross-section difference [20]. In our experiment the acceptance-averaged ratios of the kinematic coefficients of the bilinear DVCS terms to the BH-DVCS terms are below 1.2% for $d\Sigma$ and below 4.5% for $d\sigma$. By combining the contributions in Table II one obtains a precise determination of the azimuthal dependence of the $\bar{e}p \rightarrow ep\gamma$ cross section, regardless of the neglected terms in the analysis.

Our first major result is the Q^2 dependence of the $\Im[\mathcal{C}^{\mathcal{I}}]$ angular harmonics. Fig. 5 (Left) shows the results averaged over our full t domain, with $\langle t \rangle = -0.25 \text{ GeV}^2$ (varying by $\pm 0.01 \text{ GeV}^2$ over Kin 1–3). For $\Im[\mathcal{C}^{\mathcal{I}}(\mathcal{F})]$, the 3% statistical uncertainty sets an upper limit $\leq 10\%$ to twist-4 and higher contributions. This angular harmonic, $\Im[\mathcal{C}^{\mathcal{I}}(\mathcal{F})]$, is then a direct measurement of the linear combination of GPDs of Eq. 3. Fig. 5 (Right) displays the twist-2 \mathcal{C} angular harmonics of Table II (Real and Imaginary parts) as functions of t , with the predictions from a model by Vanderhaeghen, Guichon and Guidal (VGG) [26, 27, 28]. The VGG model (twist-2 contributions only, profile parameter $b_{\text{val}} = b_{\text{sea}} = 1$, Regge parameter $\alpha' = 0.8 \text{ GeV}^{-2}$, GPD $E_f = 0$) is in qualitative agreement with the $\Im[\mathcal{C}^{\mathcal{I}}(\mathcal{F})]$ data, but significantly under-predicts the principal-value integrals (\Re parts of the angular harmonics). We next note that the two twist-2 angular harmonics (Eq. 3, 5) extracted from the helicity-independent cross section $d\sigma$ determine distinct combinations of GPD integrals, with $[\mathcal{C}^{\mathcal{I}} + \Delta\mathcal{C}^{\mathcal{I}}](\mathcal{F})$ dependent only on \mathcal{H} and \mathcal{E} . This real part of the BH-DVCS interference is the same interference term that can be obtained by measurements of the difference of electron and positron (or μ^\pm) DVCS cross sections. The large contribution of the BH-DVCS interference term in

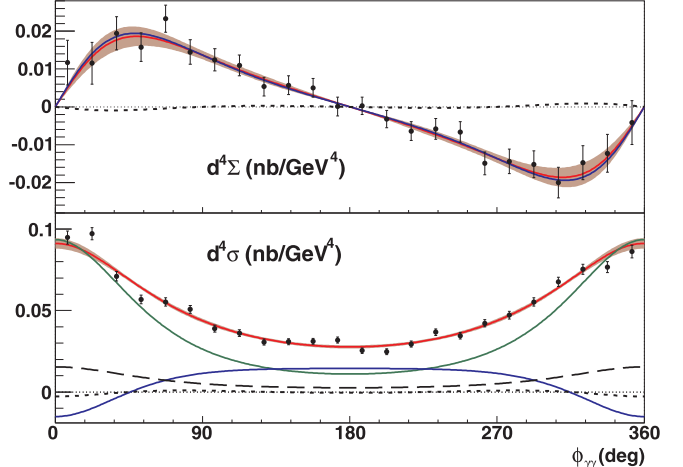


FIG. 4: Data and fit to the helicity-dependent cross section $d^4\Sigma / [dQ^2 dx_{\text{Bj}} dt d\phi_{\gamma\gamma}]$, and helicity-independent cross section $d^4\sigma / [dQ^2 dx_{\text{Bj}} dt d\phi_{\gamma\gamma}]$, as a function of $\phi_{\gamma\gamma}$. Both are in the bin $\langle Q^2, t \rangle = (2.3, -0.28) \text{ GeV}^2$ at $\langle x_{\text{Bj}} \rangle = 0.36$. Error bars show statistical uncertainties. Total fits with one- σ statistical error bands are shown in red. The systematic uncertainty is given in the text. The green line is the $|\text{BH}|^2$ contribution to $d^4\sigma$. The blue lines in $d^4\Sigma$ and $d^4\sigma$ are the contributions from the fitted $\Im m$ and $\Re e$ parts of $\mathcal{C}^{\mathcal{I}}(\mathcal{F})$, respectively. The long dashed line is the fitted $\Re e[\mathcal{C}^{\mathcal{I}} + \Delta\mathcal{C}^{\mathcal{I}}](\mathcal{F})$ term. The short dashed curves are the fitted $\Im m$ and $\Re e$ parts of $\mathcal{C}^{\mathcal{I}}(\mathcal{F}^{\text{eff}})$.

$Q^2 \setminus \langle t \rangle (\text{GeV}^2)$	$t = -0.33$	-0.28	-0.23	-0.17
$\Im m$	1.5 ± 0.3	2.1 ± 0.3	2.0 ± 0.2	3.2 ± 0.2
$[\mathcal{C}^{\mathcal{I}}(\mathcal{F})]$	1.9 ± 0.2	2.3 ± 0.2	2.5 ± 0.2	3.2 ± 0.2
	2.3 ± 0.2	2.4 ± 0.2	2.6 ± 0.2	3.3 ± 0.3
$\Im m$	1.5 ± 2.0	2.5 ± 2.0	0.1 ± 2.1	0.6 ± 2.4
$[\mathcal{C}^{\mathcal{I}}(\mathcal{F}^{\text{eff}})]$	0.3 ± 1.4	3.8 ± 1.5	-0.9 ± 1.8	4.7 ± 2.7
	2.3 ± 1.6	0.7 ± 1.8	0.2 ± 2.5	4.0 ± 4.6
$Q^2 = 2.3 \text{ GeV}^2, \Re e$ part of Angular Harmonics				
$\mathcal{C}(\mathcal{F})$	-2.4 ± 0.1	-2.0 ± 0.1	-1.7 ± 0.1	-0.7 ± 0.2
$[\mathcal{C} + \Delta\mathcal{C}](\mathcal{F})$	0.1 ± 0.1	0.8 ± 0.1	1.6 ± 0.1	2.5 ± 0.1
$[\mathcal{C}(\mathcal{F}^{\text{eff}})]$	-1.4 ± 0.5	0.6 ± 0.6	1.0 ± 0.8	3.4 ± 1.4

TABLE II: Angular Harmonics fit results, $\Im m$ and $\Re e$ parts, and their statistical uncertainties.

$d\sigma$ (Fig. 4, especially from 90° to 270°) indicates that the relative Beam Spin Asymmetry $BSA = d^5\Sigma / d^5\sigma$ cannot be simply equated to the imaginary part of the BH-DVCS interference divided by the BH cross section. Finally, these data support the prediction of perturbative QCD scaling in DVCS [1, 2], even at the modest Q^2 of this experiment. This is similar to the phenomenology of inclusive DIS results in the same x_{Bj} range [29].

We acknowledge essential work of the JLab accelerator staff and of the Hall A technical staff. This work was supported by DOE contract DOE-AC05-06OR23177

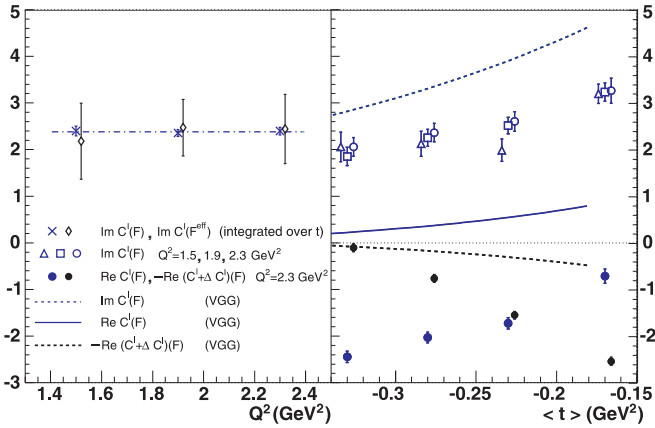


FIG. 5: Left: Q^2 dependence of $\Im m$ parts of (twist-2) $\mathcal{C}^I(\mathcal{F})$ and (twist-3) $\mathcal{C}^I(\mathcal{F}^{\text{eff}})$ angular harmonics, averaged over t . The horizontal line is the fitted average of $\Im m[\mathcal{C}^I(\mathcal{F})]$.

Right : Extracted real and imaginary parts of the twist-2 angular harmonics as functions of t . The VGG model curves are described in the text. Note the sign of $-[\mathcal{C}^I + \Delta \mathcal{C}^I](\mathcal{F})$ (data and VGG). Superposed points in both panels are offset for visual clarity. Their error bars show statistical uncertainties.

under which the Jefferson Science Associates, LLC, operates the Thomas Jefferson National Accelerator Facility. We acknowledge additional grants from the US DOE and NSF and the French Centre National de la Recherche Scientifique and Commissariat à l'Energie Atomique.

[1] X.-D. Ji, Phys. Rev. Lett. **78**, 610 (1997), hep-ph/9603249.
[2] A. V. Radyushkin, Phys. Rev. **D56**, 5524 (1997), hep-ph/9704207.
[3] D. Mueller, D. Robaschik, B. Geyer, F. M. Dittes, and J. Horejsi, Fortschr. Phys. **42**, 101 (1994), hep-ph/9812448.
[4] J. C. Collins and A. Freund, Phys. Rev. **D59**, 074009 (1999), hep-ph/9801262.
[5] X.-D. Ji and J. Osborne, Phys. Rev. **D58**, 094018 (1998), hep-ph/9801260.
[6] M. Diehl, T. Gousset, B. Pire, and J. P. Ralston, Phys.

Lett. **B411**, 193 (1997), hep-ph/9706344.
[7] M. Burkardt, Phys. Rev. **D62**, 071503 (2000), hep-ph/0005108.
[8] M. Diehl, Eur. Phys. J. **C25**, 223 (2002), hep-ph/0205208.
[9] A. V. Belitsky, X.-D. Ji, and F. Yuan, Phys. Rev. **D69**, 074014 (2004), hep-ph/0307383.
[10] A. Aktas *et al.* (H1), Eur. Phys. J. **C44**, 1 (2005), hep-ex/0505061.
[11] C. Adloff *et al.* (H1), Phys. Lett. B **517**, 47 (2001), hep-ex/0107005.
[12] S. Chekanov *et al.* (ZEUS), Phys. Lett. **B573**, 46 (2003), hep-ex/0305028.
[13] A. Airapetian *et al.* (HERMES), Phys. Rev. Lett. **87**, 182001 (2001), hep-ex/0106068.
[14] F. Ellinghaus (HERMES), Nucl. Phys. **A711**, 171 (2002), hep-ex/0207029.
[15] A. Airapetian *et al.* (HERMES) (2006), hep-ex/0605108.
[16] S. Stepanyan *et al.* (CLAS), Phys. Rev. Lett. **87**, 182002 (2001), hep-ex/0107043.
[17] S. Chen, H. Avakian, V. Burkert, and P. Eugenio (CLAS) (2006), hep-ex/0605012.
[18] J. Alcorn *et al.*, Nucl. Instrum. Meth. **A522**, 294 (2004).
[19] F. Feinstein (ANTARES), Nucl. Instrum. Meth. **A504**, 258 (2003).
[20] A. V. Belitsky, D. Mueller, and A. Kirchner, Nucl. Phys. **B629**, 323 (2002), hep-ph/0112108.
[21] A. Bacchetta, U. D'Alesio, M. Diehl, and C. A. Miller, Phys. Rev. **D70**, 117504 (2004), hep-ph/0410050.
[22] M. Rvachev, Hall A Technical Note JLab-TN-01-055, Jefferson Lab (2001), URL <http://hallaweb.jlab.org/publications/Technotes/technote.htm>.
[23] M. Vanderhaeghen *et al.*, Phys. Rev. **C62**, 025501 (2000), hep-ph/0001100.
[24] M. Baylac *et al.*, Phys. Lett. **B539**, 8 (2002), hep-ex/0203012.
[25] J. J. Kelly, Phys. Rev. **C70**, 068202 (2004).
[26] M. Vanderhaeghen, P. A. M. Guichon, and M. Guidal, Phys. Rev. **D60**, 094017 (1999), hep-ph/9905372.
[27] K. Goeke, M. V. Polyakov, and M. Vanderhaeghen, Prog. Part. Nucl. Phys. **47**, 401 (2001), hep-ph/0106012.
[28] M. Guidal, M. V. Polyakov, A. V. Radyushkin, and M. Vanderhaeghen, Phys. Rev. **D72**, 054013 (2005), hep-ph/0410251.
[29] S. Eidelman *et al.* (Particle Data Group), Phys. Lett. **B592**, 1 (2004), URL pdg.lbl.gov.